Tissue Safety Analysis and Duty Cycle Planning for Galvanic Coupled Intra-body Communication

Meenupriya Swaminathan, Ufuk Muncuk and Kaushik R. Chowdhury,
Electrical and Computer Engineering Department, Northeastern University, Boston, MA 02115, USA.
E-mail:{meenu, muncuk.u, krc}@ece.neu.edu.

***Abstract*—Galvanic coupling is the enabler of closed-loop communication between implanted sensors and embedded actuating devices (such as drug injectors) by providing energy-efficient and reliable non-RF transmission through links formed within tissue. For safe deployment, it is critical to verify that the amount of heat generated within tissues during signal propagation stays within permissible bound. In this paper, we analyze the thermal distribution within tissues, for galvanic coupling-based communication for varying transmission power levels, number of collocated transmitters, and blood perfusion conditions using finite element based numerical simulation and skin-phantom based experiments. Our results confirm that tissue heating remains well below safe limit of $1\,^{\circ}C$. Using the temperature dissipation profile, we derive the suitable transmission duty cycles, separation distances and number of concurrent sources that may co-exist without raising the tissue temperature. The proposed strategies provide upto four fold increase in bandwidth efficiency through concurrent transmissions, ensuring sufficient bandwidth for implant communications.**

I. Introduction

Implanted sensors monitor critical internal body factors, such as oxygen saturation, arterial pressure, hormone levels and renal functions, among others, and accordingly provide inputs for adjusting the drug delivery volumes, or activate embedded actuators, such as neural stimulators. Realization of these functions require direct communication among implants through the body tissues, which is difficult to achieve using conventional radio frequency (RF) waves owing to their high attenuation through the body tissues. As an alternate to the RF waves, galvanic coupling (GC) can be used for intra-body communication [1] that induces a field well below the permissible limit of $25\,\mathrm{mW/m^2}$ [2], and uses weak electrical current to propagate through conducting body tissues.

GC based tissue communication works best within the range $100\,\mathrm{kHz}$ to $1\,\mathrm{MHz}$, which is higher than the body's natural neuro-electrical activity frequencies, and offers lower energy absorption in tissues. However, the principal side effect arising from signal propagation in tissues in this KHz frequency range is tissue heating. Rise in local tissue temperature upto $1\,^{\circ}C$ is safe, as it can be easily controlled by the body's natural thermo-regulation system [2]. The main result of this paper is that the weak signal power used in a typical two-node GC link of length $15-20\,\mathrm{cm}$, i.e., a $5\,\mathrm{mA}$ source signal results in a temperature rise that is much lower than $1\,^{\circ}C$.

We envision that multiple sensors and actuators, possibly forming an array of electrodes, may be embedded in the tissue for long term holistic monitoring, and many of them may exist in close proximity. This situation raises the following concerns: (i) When there are multiple long-term concurrent sources, the aggregated signal level may inject more thermal energy than what can be safely handled, (ii) When the variable blood perfusion rate, i.e., the primary body temperature regulating factor, drops below to a very low value, the increase in the local tissue temperature may impact the core body temperature.

To address these concerns, accurate knowledge of tissue thermal distribution is required that will also enable planning of transmission duty cycles and sequences. In this paper, we use finite element based numerical analysis to study the thermal distribution when signal propagates through the tissues. This study, accompanied by experimental measurements and duty cycle selection approach, also helps to capture the otherwise *rare* real-life situations, such as reduced or high rate blood flow, and the resulting impact on tissue temperature in the presence of concurrent transmissions from several closely located sources. Our major contributions in this paper are as follows:

a) We analyze the thermal distribution in tissues in the presence of single or multiple sources and demonstrate that the net temperature rise remains below $1^{\circ}C$, which can then be efficiently regulated by the body's natural mechanism.

b) We investigate the sensitivity of the spatio-temporal temperature profile in association with the normal and extreme rates of blood perfusion.

c) We devise optimized duty cycles for the implanted sensors and a transmission sequencing policy to control the temperature increase, as well as to improve the per-node bandwidth efficiency.

The paper is organized as follows. Sec.II presents the GC tissue heating model. Sec.III, introduces the effects of varying perfusion and suggests appropriate duty cycles and transmission sequences. Sec.IV summarizes the results of the simulation and empirical test beds and Sec.V concludes the paper.

II. Tissue Heating Model for Galvanic Coupling

In this section, we develop a model that will enable analyzing the spatio-temporal thermal distribution in the presence of single or multiple galvanic coupled transmitters.

A. Related Work and Preliminaries

Tissue heating caused by medical procedures such as diathermy, RF ablation, MRI and ultrasound procedures [3]

have been extensively studied in the past. Similarly, heating effects of implants have been investigated in the high frequency range [6] and in the MHz and GHz frequency range [4] for understanding the Specific Absorption Rate (SAR) from the radiation effects. In the range 100 kHz to 1 MHz, tissues have higher conductivity and offer longer signal propagating paths. Owing to this reduced attenuation, and hence absorption, the rise in temperature is also on the lower side. While the tissue heating effect of the higher kHz range has been analyzed for high power applications such as Diathermy, the impact of low power galvanic coupled links with possible multiple concurrent transmitters has not yet been studied.

We use the modified form of the classical Pennes Bioheat equation [5] for analyzing the heat generated in resting forearm, in which the rate of spatial tissue heat accumulation is given by

$$\rho_i C_i \frac{\partial T}{\partial t} = \nabla . k_i \nabla T + Q_{src} - Q_b \tag{1}$$

where ρ, C and k are the thermal properties namely density, specific heat and thermal conductivity, $\frac{\partial T}{\partial t}$ is the rate of thermal variation, $\nabla . k_i \nabla T$ is the heat flux, Q_{src} denotes the thermal sources and Q_b indicates the thermal regulation by blood perfusion. Subscript i indicates properties of a specific tissue i.

B. Metabolic & GC Transmitter Heat Source Model (Q_{src}):

Tissues that have an embedded GC transmitter also have various ambient sources of heat. The normal body temperature is regulated using the metabolic heat generated by tissues with a rate of generation Q_m that varies based on the tissue type, part of the body, ambient temperature and activity level. When a GC transmitter embedded in tissue injects a signal in the frequency range of 100 kHz to 1 MHz, a flow of current is induced in the form of conductive power dissipation. The work done in overcoming the tissue impedance during the current flow is converted to heat at a rate Q_{cndc}. Thus, the specific value of Q_{cndc} at a point in the tissue depends on the injected signal strength and the tissue channel gain. When an electrode positioned at a point A injects the signal, we estimate the signal strength observed at point B using the channel gain g_{AB} obtained from our earlier work in developing tissue channel models in [1].

The dielectric nature of tissue gives rise to dielectric power dissipation with a heat generation rate Q_{diel}, which is caused by the molecular dipole rotation. While this phenomenon is significant in the GHz frequency range, the contribution of Q_{diel} in the low kHz, as is used by galvanic coupled tissues, is negligible, especially when compared to the dominant component of Q_{cndc}. The aggregated rate of conduction and dissipation of heat generated at a point B by a GC transmitter at point A can be expressed as

$$Q_{cndc} + Q_{diel} = k_s(\sigma_i(w) + jw\epsilon_i(w))P_{in}.g_{AB}, \tag{2}$$

where P_{in} is the power admitted at the electrodes, σ_i is the conductivity of tissue i, $w = 2\pi f$ is the angular frequency, f is the frequency and ϵ_i is the tissue permittivity. When multiple transmitters coexist in a given area of a tissue with non-negligible co-interference, the total heat generated can be computed from the aggregated power level, given by,

$$Q_{cndc}{+}Q_{diel} = k_s(\sigma_i(w){+}jw\epsilon_i(w)) \sum_N (P_{in} g_{AB}) \tag{3}$$

With the metabolic, conductive and dielectric sources of thermal generation, Q_{src} in (1) can be expressed as

$$Q_{src} = Q_m + Q_{cndc} + Q_{diel} \tag{4}$$

C. Impact of Blood Perfusion on GC Tissue Heating (Q_b)

Perfusion is the rate of heat transfer between the tissue and the arterial blood stream that plays a critical role in determining the steady state tissue temperature. The blood perfusion Q_b is expressed in terms of temperature difference between the tissue and blood given by

$$Q_b = w_b \rho_b C_b (T - T_a) \tag{5}$$

where w_b is the blood flow rate, ρ_b and C_b are the density and specific heat capacity of blood and T_a is the arterial blood temperature.

D. Impact of Boundary conditions on GC Tissue Heating:

The thermal sources and sinks that are specifically deployed at certain surfaces (e.g., convection at the air-tissue interface) and parts of tissue (e.g., heat flux at electrode-tissue interface) can be modeled as individual boundary conditions as follows:

• Tissue-tissue interface: We assume zero heat flux at the boundaries that connect the tissue under study with other tissues, which when stated as zero Neumann boundary, takes the following form:

$$\overrightarrow{n} . k_i \nabla T + qT = g \tag{6}$$

where the parameters q & g are set to 0 and $\overrightarrow{n}$ is the unit normal vector.

• Convection at air-tissue interface: The temperature at the skin surface exposed to air is influenced by the ambient temperature. We model the boundary condition at the air-tissue interface as the convectional heat exchange, which according to the Newton's law of cooling is given by

$$k_s \frac{\partial T}{\partial x} = h_{cnvc}(T_{amb} - T) \tag{7}$$

where h_{cnvc} is the convection coefficient. The corresponding Neumann boundary in (6) has $q{=}h_{cnvc}$ and $g{=}h_{cnvc}T_{amb}$.

• Electrode-tissue interface: The heat generated inside the sensor nodes, the transceiver circuits and the electrodes are also dissipated to the surrounding tissue according to the classical Fourier's law. We model this source of heat as a Dirichlet boundary heat source q_{circ} at all the five electrode faces in contact with the tissue given by,

$$q_{circ} = k_e(\sigma_e P_{in} + T_n) \tag{8}$$

where k_e, ρ_e and C_e are the thermal properties of electrode, σ_e is the electrode conductivity and T_n is the temperature generated inside the node circuitry.

We use the model presented here for studying the tissue thermal response when coupled to an embedded signal source.

III. Duty Cycle and Sequencing based Thermoregulation

Under the normal conditions, the thermal energy induced in tissue from GC transmission is close to the negligible amount (see Fig.5(a)) as the induced power is below the safe limit suggested by [2] and the induced thermal energy is at least two orders of magnitude lower than the suggested safe level of $1\,^{\circ}C$. However, in rare physiological conditions, the perfusion (w_b) may reach extreme values beyond the average maximum w_b^{max} and minimum w_b^{min} values. Moreover, multiple transmitters can be embedded close to each other and engage in concurrent transmissions. We consider three of such conditions in this section and devise appropriate duty cycles and transmission sequence.

Poor Perfusion Effect: Under critical situations such as tissue damage, arterial damage or development of pressure points from prolonged resting, w_b drops too low to quickly regulate the local tissue temperatures. This results in accumulation of thermal energy at points close to or in contact with the transmitting electrodes. When w_b drops to a low value, less than w_b^{min}, the medium access should be controlled to keep the local temperature elevation within bounds, particularly when there is no perfusion as discussed below.

• *Zero Perfusion:* When w_b=0, the temperature elevates steeply with a high rate, reaching steady state at t=∞. In such state of perfusion, the local temperature elevation can be controlled by transmitting (t_{ON}) for very short period (e.g., $0.1\,$secs) with long Inter Transmission Pause (ITP) period, t_{OFF} ($\approx 1\,$min). The short t_{ON} and long ITP phase offers a low bandwidth efficiency (η) computed as $\frac{t_{ON}}{t_{ON}+t_{OFF}}$. When there are concurrent transmissions, each transmission elevates the temperature of the entire tissue area under study (refer Fig.4(b)). Therefore, concurrent transmissions are not recommendable when w_b=0. Possibly, each node can take turns in utilizing the brief t_{ON} for signaling emergency link down state caused by poor perfusion. Sharing of the narrow bandwidth among multiple transmitters further plummets the bandwidth efficiency per node (η), down as

$$\eta = \frac{1}{N}\frac{t_{ON}}{t_{ON}+t_{OFF}}, \quad \eta_{all} = \frac{t_{ON}}{t_{ON}+t_{OFF}} \tag{9}$$

where N is the number of collocated nodes and η_{all} is the bandwidth efficiency offered in total for all N nodes.

• *Non-zero Poor Perfusion:* For $0<w_b<w_b^{min}$, the time required for bringing the elevated temperature to base body temperature (T_{base}) is much less than that required for the zero perfusion state (≈ 5 to $10\,$secs from Fig.5(e)). Moreover, the temperature elevation is higher in the electrode neighborhood and gradually drops with the channel gain g i.e., the temperature elevation for larger distances from electrode is negligible. We denote the maximum distance from electrode experiencing noticeable rise in temperature as D_T. These features can be leveraged towards improving η as follows:

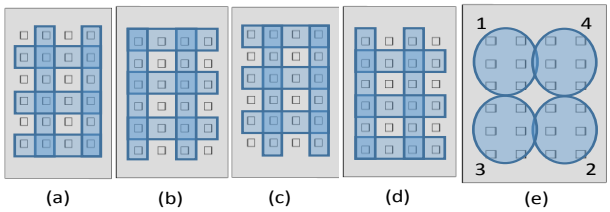

Fig. 1. Transmission sequence for multiple transmitters

1. Duty Cycle Based Control: Long term exposure to elevated temperature would impact the global body temperature. Hence we set our primary objective in the poorly perfused tissue to control the period of exposure, t_{ON} to a target temperature T_{target}. We use the net spatio-temporal local tissue temperature elevation (T_{net}) as a parameter to control the level of thermal exposure, computed as:

$$T_{net} = \int_{t_1}^{t_2}\int_{V} T dV dt < T_{target} \tag{10}$$

for $t_{ON} \in [t_1, t_2]\,$secs, where, V is the spatial domain. T_{target} generally depends on w_b, h_{cnvc} and tissue area (e.g., ankle or abdomen). When $T_{net} \geq T_{target}$, we pause the transmission with ITP phase. This approach would nullify any noticeable influence of the local temperature over the global temperature and would also enable longer t_{ON} phases for single transmission case.

2. Duty cycle & Concurrency Control: The above strategy can be extended to concurrent multiple transmissions ($m \leq N$) if $T_{net} \leq T_{target}$ with the t_{ON} periods of all the m transmitters coinciding. When T_{net} exceeds T_{target}, the ITP phase ensues to bring $T_{net} = 0$ and then the cycle repeats. The per node and the total bandwidth efficiency in this case is improved from (9) by a factor m as

$$\eta = \frac{m}{N}\frac{t_{ON}}{t_{ON}+t_{OFF}}, \quad \eta_{all} = \frac{m^2}{N}\frac{t_{ON}}{t_{ON}+t_{OFF}} \tag{11}$$

The above defined concurrent strategy can be realized by leveraging the electrode spatial diversity to distribute the local temperature rise evenly in the tissue. For instance when two concurrent transmissions are not sufficiently separated they would influence each other, i.e., if the first transmitter is in the ITP phase and the second transmission is ongoing, the temperature in the area between the first and second transmitters cannot reach T_{base} (refer Fig.5(d) in Sec.IV). To avoid this neighborhood effect, the concurrent transmitters should be spatially well separated, with distance greater than D_T. We formulate this condition as $x.d_{es}+y.d_e \geq D_T$, where d_{es} is the electrode separation distance, d_e is the electrode dimension, (a,b) & (c,d) are the row and column location of the electrodes 1 & 2 respectively, x=$\sqrt{(a\text{-}c)^2+(b\text{-}d)^2}$ and y=$\sqrt{(a\text{-}c\text{-}1)^2+(b\text{-}d\text{-}1)^2}$. For e.g., the distance between the electrodes in (1,1) and (5,1) in Fig.2(c) is given by $4d_{es}+3d_e$. A possible sequencing strategy is depicted in Fig.1(e), where if the first cycle transmits from region 1 and then the second cycle should choose a node from the region 2 that is diagonally farther from the first transmitter. The third cycle should choose from the region 3 and so on.

Very High Perfusion Effect: High perfusion with $w_b > w_b^{max}$ indicates a state of tissue abnormality, possibly caused by any one of a multitude of factors such as infection, vasodilation and high blood pressure. During such conditions, a local tissue temperature rise would push up the perfusion rate further, aggravating the situation. To control this, we restrict t_{ON} to a duration that bounds $T<50\%$ of its steady state value, followed by the ITP phase. Very high values of w_b offers short duration of both t_{ON} and t_{OFF} (refer Fig.5(e)). Hence, better control of the temperature elevation can be obtained with quickly alternating t_{OFF} and t_{ON} phases enabling better bandwidth efficiency compared to the poor perfusion state (refer Table.II). Multiple concurrent transmitters in tissues with $w_b > w_b^{max}$ should share t_{ON} among themselves to control the overall rise in local temperature, bringing down the per node bandwidth availability as in (9).

Temperature Control with Normal Perfusion: When w_b is within the average limits, the temperature rise in the area surrounding the electrode reaches a steady state in a few seconds (refer Fig.5(a) & (b)) that is in the safety limits. Also, the t_{OFF} duration is shorter than the poor perfusion state. Hence, the medium can be accessed with extended t_{ON} phases and shortened ITP phases. On this basis, we modify the duty cycle & concurrency control strategy proposed for non-zero poor perfused tissue as follows to further improve the per node bandwidth efficiency.

• *Reduced ITP phase:* Rather than waiting for the elevated temperature to drop to T_{base}, a transmitter can start its t_{ON} phase when the temperature of the neighbor drops to 10% of the elevated value. This would significantly increase η as the last 10% fall in temperature takes more than 25% of the total t_{OFF} duration (refer Fig.5(e)). This residual temperature would eventually fall to T_{base} in the next ITP phase that follows the t_{ON} phase of its neighbor. The per node bandwidth efficiency and all node bandwidth efficiency in this case are given by

$$\eta = \frac{t_{ON}}{n(t_{ON}+0.75\,t_{OFF})}, \quad \eta_{all} = \frac{m}{n}\frac{t_{ON}}{(t_{ON}+0.75\,t_{OFF})} \tag{12}$$

where $n \leq N$ is the number of transmitters in a neighborhood with distance of separation less than D_T. We analyze this strategy in Sec.IV using Fig.5(c).

• *Skipped ITP phase:* The minimum temperature elevation with normal perfusion can be exploited with successive t_{ON} phases as illustrated in Fig.5(d) for the n closely located transmitters. This successive transmission can be used in conjunction with the distant concurrent m transmitters discussed in the non-zero poor perfusion state. The ITP phase follows the n t_{ON} phases. During ITP phase, all the points reach T_{base}, ensuring good thermoregulation as well as improved η.

For instance, for a 24 transmitter grid in Fig.1, during the first t_{ON} phase, the unshaded 6 transmitters in the first (left most) pattern transmit. Next we choose the 6 unshaded transmitters in the next pattern in Fig.1(b) that are located diagonally to the initial set of transmitters. This would enable the local temperature in the initial transmitters to lower ensuring T_{net} to be below T_{target}. η in this case can be very high compared to any of the above mentioned strategies because of m parallel t_{ON} sessions and all N transmitters sharing a single ITP phase:

$$\eta = \frac{t_{ON}}{nt_{ON}+t_{OFF}}, \quad \eta_{all} = \frac{mt_{ON}}{nt_{ON}+t_{OFF}} \tag{13}$$

Duty Cycle Policy: Based on the above discussion, our fitted duty cycle control policy on t_{ON} & t_{OFF} is summarized below for a specific scenario for the parameters in Table.II.

$$t_{ON} = \begin{cases} t_{min}, & \forall w_b \leq w_b^{min} \\ 7.206 - \frac{1.164}{\sqrt{w_b}}, & \forall w_b^{min} < w_b \leq w_b^{max} \\ 0.72 - 0.2w_b, & \forall w_b > w_b^{max} \end{cases} \tag{14}$$

$$t_{OFF} = \begin{cases} 1.7w_b^2 - 6.3w_b + 6.74, & \forall w_b \leq w_b^{min} \\ 0.4w_b^2 - 2.8w_b + 6.4, & \forall w_b^{min} < w_b \leq w_b^{max} \\ t_{max}, & \forall w_b > w_b^{max} \end{cases} \tag{15}$$

We analyze these policies along with the thermal distribution results, duty cycle and sequencing strategies as well as the bandwidth efficiency achieved in the following section.

IV. Simulation Results and Experimental Studies on GC Thermal Distribution

In this section, we explain our finite element based numerical simulation and skin phantom-based empirical approach for investigating the transmission duty cycle effects on tissue thermal distribution.

Finite element based simulation set-up

We model the three dimensional rectangular tissue slab of dimension $15 \times 20 \times 0.3\,\mathrm{cm}^3$ using Autodesk 123D Design software. A cubical volume of dimension $1 \times 1 \times 0.05\,\mathrm{cm}^3$ is carved out of the tissue block to mark the site of the electrode. We build the one electrode, two electrode and multielectrode models as illustrated in Fig.2(a),(b) and (c) respectively. In the multielectrode model, the electrodes are separated by $2.3\,\mathrm{cm}$. Each electrode has five faces if on surface and six faces in case implanted. We import the model geometry to MATLAB, generate and redefine the tetrahedral mesh for finite element analysis as shown in Fig.2(d). The spatio-temporal thermal energy distribution in the model is obtained by solving (1) using the parabolic PDE solver over a given period of time. We set the parameter as given in Table.I with the boundary conditions set individually as required for different conditions.

1. Model verification: Initially, we verify the steady state tissue temperature to be maintained at $T_{base} = 35\,^{\circ}C$, without the external signals. The electrode faces $F1$ to $F5$ in Fig.2.(a) are set as insulating boundaries. We apply (7) to the tissue face $F6$ to make it act as a convective boundary and assume that Q_{src}=Q_m. The resulting steady state temperature through out the tissue is within $35 \pm 10^{-12}\,^{\circ}C$ as shown in Fig.3(a), thus ensuring accurate thermo-regulation of the tissue. It takes around $2\,\mathrm{secs}$ for the simulator to reach the steady state

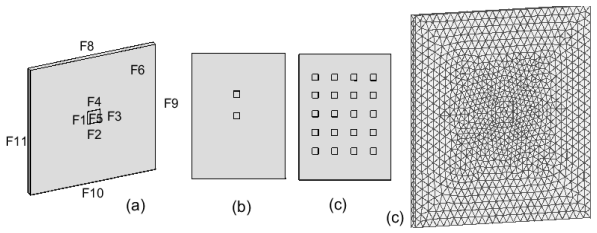

Fig. 2. 3D models (a) one source with face numbers displayed (b) two sources (c) multiple (20 sources) and (d) the relaxed mesh for (a)

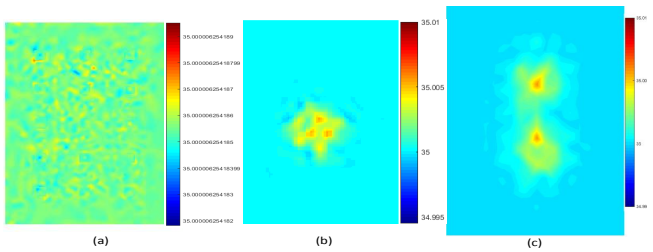

Fig. 3. Thermal distribution for $P_{in} = 10\,\mathrm{mW}$ at face $F7$ for (a) No transmission (b) 1 transmission and (c) 2 concurrent transmissions

temperature. We therefore, allow $2\,\mathrm{secs}$ as the initial phase in each simulation procedure.

2. Thermal Distribution vs Transmit Power: To observe the tissue temperature variation during a transmission, we alter the boundary condition of the electrode faces (face $F1$ to $F5$ in Fig.2(a)) as constant heat flux (8). For this analysis, Q_{src} takes the form in (4) to include the conductive and dissipative effect (2) of the current flowing through the tissue. Fig.3(b) shows the spatial temperature profile for P_{in}=10 mW after $10\,\mathrm{secs}$ at the non-convective side (face $F7$, behind $F6$), which experiences higher temperature elevation compared to the convective face. The temporal thermal elevation is depicted in Fig.5(a) for P_{in}=1 mW, 10 mW and 100 mW and w_b=1.2 at points that are $0.5\,\mathrm{cm}$ and $2\,\mathrm{cm}$ away from the electrode. The maximum temperature is recorded at the area in contact with the electrode followed by the points in $F7$ that are directly behind the contact area. The elevation in temperature is present only at the proximity of the electrode within an average radius, D_T of $3\,\mathrm{cm}$ at the convective face and $3.5\,\mathrm{cm}$ at the non-convective face, that reaches steady state in few seconds.

3. Empirical validation using Skin Phantom: We validate the tissue thermo-regulation model explained above using a skin phantom ($7 \times 7 \times 0.3 \times \mathrm{cm}^3$) coupled with 2 sources. The experimental set-up is shown in Fig.4(a). We use the alligator clips (40 mm) as the exciting and ground electrodes and a high precision RTD thermometer to measure the rise in temperature. We modify the simulation model parameters (such as the tissue, electrode dimensions) with $w_b = 0$ to match with the phantom set-up.

We compare the temperature generated in the phantom for a 1 mW signal with that of the corresponding simulation model in Fig.5(g) upto $50\,\mathrm{min}$. we observe that the temperature rise is linear in both simulation and experiment, with a slightly faster rate of rise in phantom. This is caused by deeper signal injection to the tissue through the sharp pins in the aligator clips while the simulation uses a flat surface electrode geometry. The close match in thermal distribution between the simulated and empirial set-up validates the proposed finite element model used for the analyses in this paper.

TABLE I
SIMULATION PARAMETERS, WHERE S-SKIN B-BLOOD E-ELECTRODE

Parameter	Value	Parameter	Value
Frequency (f in kHz)	100	Circuit temp. ($T_n\,^\circ C$)	0.01
Convection coeff (h_{cnvc})	3	T_{target} ($^\circ C$)	20
Ambient temp. ($T_{amb}\,^\circ C$)	25	Body temp. ($T_{base}\,^\circ C$)	35
S density [kg/m^3]	1040	S specific heat [J/kg°C]	3600
S thermal conduct[W/m°C]	0.32	Metabolic heat (Q_m)	55
B density [kg/m^3])	1600	B specific heat [J/kg°C]	3960
B thermal conduct[W/m°C]	0.49	E specific heat [J/kg°C]	134
E thermal conduct[W/m°C]	31	E conductivity[s/m]	4e6
E density [kg/m^3]	2.2e4		

4. Two Concurrent Transmissions: Next, we extend this model for two concurrent transmissions by adding the constant heat flux (8) for two electrodes in Fig.2(b). The Q_{src} term in (4) uses the conduction and dissipation effect in (3) for incorporating both the current sources in the computation. The spatial distribution of T after $10\,\mathrm{secs}$ at the non-convective side is shown in Fig3(c), which has the maximum temperature rise same as that of the single transmission case. However, when the two electrodes are separated less than $3\,\mathrm{cm}$ ($2.3\,\mathrm{cm}$ in Fig3(c)), the heat density in the area between the two electrodes is higher than the rest of the surrounding tissue because of the heat aggregation. Fig.5(b) shows the temporal thermal elevation for P_{in}=1 mW, 10 mW and 100 mW and w_b=1.2 at $0.5\,\mathrm{cm}$ (position A), $1\,\mathrm{cm}$ from electrode 1 towards the edge (position C) and at the mid point between the electrodes (position B). Note that at B, which is $0.15\,\mathrm{cm}$ farther from electrode 1 than C, the generated heat is atleast $0.01\,^\circ C$ higher, proving that separation between concurrent transmissions is a key factor in determining the local temperature rise.

5. Thermal Distribution vs Perfusion: In Fig.5(e) the steady state temperature for w_b=1.6 is reached in $<1\,\mathrm{secs}$ while that for w_b=0.4, takes $\approx 9\,\mathrm{secs}$. The worst case (w_b=0) is depicted in Fig.5(g), where the temperature with 2 sources reach the $1\,^\circ C$ in $6.6\,\mathrm{hours}$, exceeding the safe limit. Fig.5(f) compares T_{net} computed using (10) versus the number of concurrent transmitters in a tissue area over $20\,\mathrm{secs}$ when w_b is within the average limits for P_{in}=1 mW. For $T_{target} = 20\,^\circ C$, the safe number of concurrent transmissions can go upto 9.

- *Reduced ITP phase:* Fig.5(c) illustrates the duty cycle

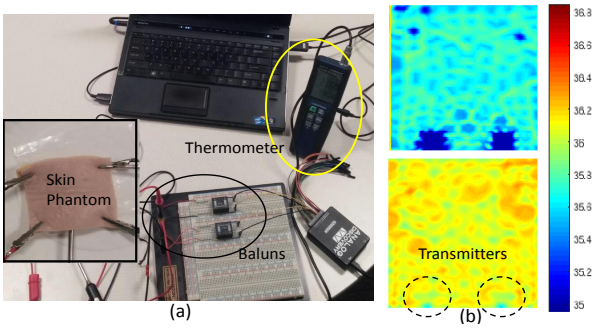

Fig. 4. (a) Empirical set-up with skin phantom & 2 transmitters (b) Simulated spatial thermal profile ($^\circ C$) after $5e4\,\mathrm{secs}$

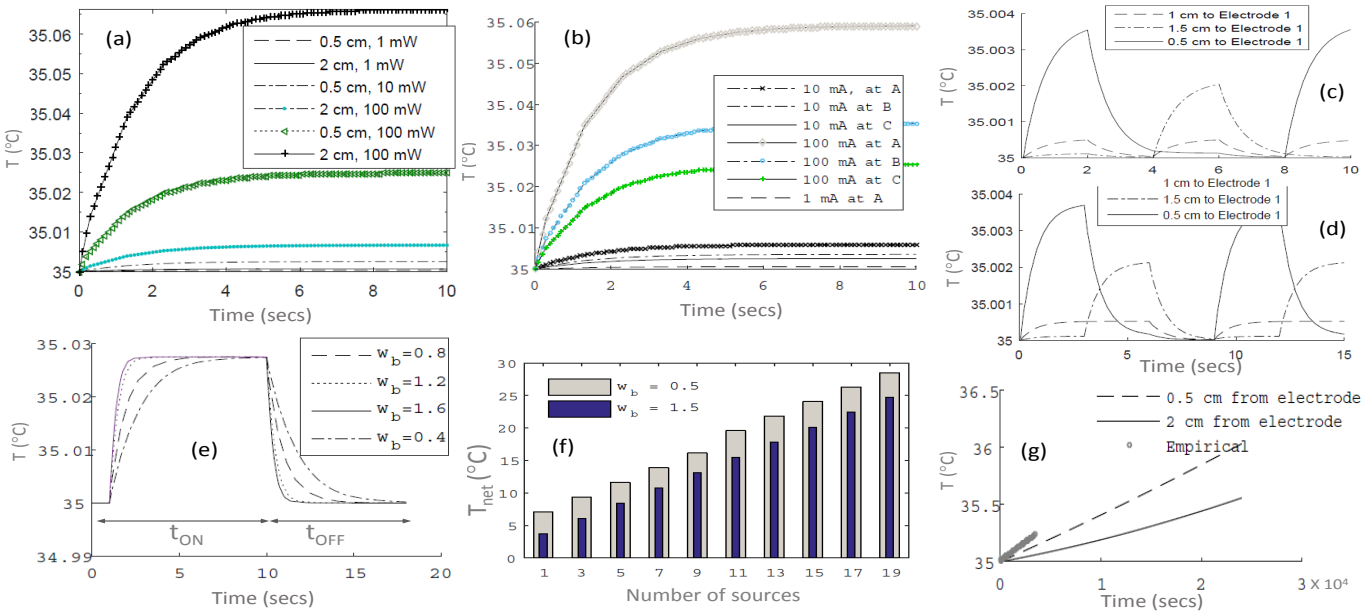

Fig. 5. (a) Rise in Temperature ($^{\circ}C$) with varying P_{in} for 1 transmitter and (b) for 2 transmitters (c) Reduced ITP for 2 transmitters; (d) Skipped ITP for 2 transmitters (e) t_{ON} & t_{OFF} vs w_b; (f) T_{net} vs number of concurrent transmissions; (g) T for $w_b = 0$ and model validation using phantom experiment.

based thermoregulation for 2 transmissions. The temperature rises more at $0.5\,\mathrm{cm}$ from electrode 1 than at farther points during t_{ON}=$[0, 2]$ $secs$ and then drops to 90% of t_{base} during the next t_{OFF}=$[2, 4]$ secs. During t_{ON}=$[4, 6]$ $secs$, electrode 2 transmits rising the temperature near electrode 2 and in between the 2 electrodes. However, the temperature at point closer to electrode 1 continue to drop and reaches t_{base} in the next t_{OFF} slot. This technique improves the per node efficiency by atleast 10%.

• *Skipped ITP phase:* Fig.5(d) displays the temperature control when the first ITP phase after the t_{ON} of electrode 1 is occupied by the t_{ON} of electrode 2. In the following ITP phase, all the points reach T_{base}, ensuring good temperature control and improves η by atleast 3.5% and η_{all} by 13% more than the Reduced ITP strategy. Table.II summarizes bandwidth efficiencies obtained using skipped ITP phase for average perfusion state.

V. Conclusion

While GC communication technology has the potential to revolutionize personalized implant-based sensing and help realize the connected healthcare vision, it must operate within various safety thresholds. The tissue thermal analysis presented in this paper demonstrates that GC provides safe operating conditions with the temperature elevation in normal tissue conditions restricted within bounds. By appropriately adjusting the duty cycles and sequence of concurrent transmissions, we have demonstrated the GC can operate with high reliability, better bandwidth efficiency, and is adaptable to the abnormal tissue conditions. While we have connected the tissue heating profiles with duty cycles, our next efforts will be directed towards a complete medium access protocol for both contention- and polling-based implants.

TABLE II
DUTY CYCLE & BANDWIDTH EFFICIENCY (t_{min}=0.1 secs, t_{max}=2.2 secs, T_{target}=20 $^{\circ}C$, w_b^{min}=0.5 & w_b^{max}=1.5, $m = 4, n = 6$)

State	w_b	t_{ON}	t_{OFF}	η (N=1)	η (N=24)	η_{all}
	0	0.1s	50s	0.2%	0.01%	0.2%
Poor	0.1	0.1s	7s	1.43%	0.24%	0.96%
Perfusion	0.3	0.1s	6.2s	1.6%	0.27%	1.08%
Average	0.6	5.7s	5.6s	50.4%	14.3%	57.3%
Perfusion	1.0	6.05s	3.36s	64.3%	15.3 %	61%
	1.4	6.4s	3.3s	66%	15.4%	61.4%
Very high	1.6	0.4s	2.2	15.38%	0.64%	0.64%
Perfusion	2.0	0.32s	2.2	12.7%	0.53%	0.53%

Acknowledgment

This material is based on the work supported by the U.S. National Science Foundation under Grant No. CNS-1453384.

References

[1] M. Swaminathan, F. S. Cabrera, J. S. Pujol, U. Muncuk, G. Schirner, and K. R. Chowdhury, "Multi-path model and sensitivity analysis for galvanic coupled intra-body communication through layered tissue," *IEEE Transactions on Biomedical Circuits and Systems*, 2015.

[2] P. Vecchia, R. Matthes, G. Ziegelberger, J. Lin, R. Saunders, and A. Swerdlow, "Exposure to high frequency electromagnetic fields, biological effects and health consequences (100 khz-300 ghz)," *International Commission on Non-Ionizing Radiation Protection*, 2009.

[3] L. Maggi, T. Omena, M. Von Krueger, and W. Pereira, "Didactic software for modeling heating patterns in tissues irradiated by therapeutic ultrasound," *Brazilian Journal of Physical Therapy*, vol. 12, no. 3, 2008.

[4] B. Ilie and D. Rafiroiu, "Experimental and computational study of the temperature distribution at the surface of a metallic implant exposed to high frequency electromagnetic fields," in *Conference on Advancements of Medicine and Health Care through Technology*, 2014, pp. 295–300.

[5] H. H. Pennes, "Analysis of tissue and arterial blood temperatures in the resting human forearm," *Journal of applied physiology*, vol. 1, no. 2, pp. 93–122, 1948.

[6] Wainwright, P R, "The relationship of temperature rise to specific absorption rate and current in the human leg for exposure to electromagnetic radiation in the high frequency band." Physics in medicine and biology, 48(19), p - 3143, 2003.